Optical Materials 122 (2021) 111728

Contents lists available at ScienceDirect

Optical Materials

journal homepage: www.elsevier.com/locate/optmat

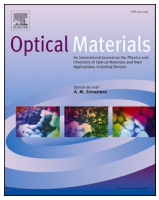

Laser induced surface enhanced Raman scattering of silver thin films decorated with carbon nanoparticles

Qianbing Cheng [a], Qingyou Liu [b], Yikai Jiang [a], Guohao Xia [a], Ruijin Hong [a,*], Chunxian Tao [a], Qi Wang [a], Hui Lin [a], Zhaoxia Han [a], Dawei Zhang [a]

[a] Engineering Research Center of Optical Instrument and System, Ministry of Education and Shanghai Key Lab of Modern Optical System, University of Shanghai for Science and Technology, No.516 Jungong Road, Shanghai, 200093, China
[b] Key Laboratory of High-temperature and High-pressure Study of the Earth's Interior, Institute of Geochemistry, Chinese Academy of Science, Guiyang, 550081, China

ARTICLE INFO

Keywords:
Carbon nanoparticles
Ag/C thin film
SPR
SERS
FDTD

ABSTRACT

Silver (Ag) thin films decorated with carbon nanoparticles were achieved by ablating Ag/C thin film with an Nd: YAG fiber pulsed laser under the environmental conditions. The structure and optical properties of the Ag/C samples were investigated. In this study, the Surface plasmon resonance (SPR) wavelength of Ag/C samples shift from 457 nm to 527 nm was realized using a different laser scanning rate. Compared to Ag samples, Surface enhanced Raman scattering (SERS) of Ag/C samples was also observed due to decorating with nano-carbon, which demonstrates good steadiness and high SERS intensity with the concentration of Rhodamine 6G (Rh 6G) with 10^{-5} mol/L. In additional, the simulation results of finite-difference-time-domain (FDTD) verify SERS performance.

1. Introduction

Since the 1970s, with the development of science and technology, SERS detection sensitivity has gradually increased, and the technology application has also continued to develop [1–3], and it has been widely used in various fields such as physics, chemistry, materials, and biomedicine [4,5]. Recent decades, with the emergence of plasma Au, Ag, Cu and transition metal nanomaterials, the research and application of Raman spectroscopy have attracted renewed interest [6,7]. At present, the SERS effect mainly has two mechanisms: electromagnetic enhancement (EE) and chemical enhancement (CE) [8,9]. In general, electromagnetic enhancement is dominants and is mainly related to the extensive local field caused by LSPR [4,10,11]. Therefore, the prerequisite for metal nanoparticles to have excellent SERS performance is that they have good LSPR properties.

Precious metals such as Au and Ag are ideal plasma materials for the SERS substrate preparation because of their excellent chemical properties [12–14]. Ag is an ideal SERS active matrix material because of its powerful and adjustable LSPR in the visible to near-infrared spectrum [15]. However, these materials have not been widely used in SERS substrates due to silver being easily oxidized susceptible to fluorescence interference from the detected substance during the test [16–18]. Besides, Ag and semiconductors' composite structure can solve easy oxidation, but the complexity of its manufacturing process still limits its development [19,20]. Graphene is known to have excellent optical, electrical and mechanical properties. The composite structure of graphene and metal NPs has the advantage of simultaneously combining magnetic and chemical enhancement in a single substrate [13,21–23]. Moreover, graphene has an excellent fluorescence quenching effect. The mechanism is that the fluorescence of the fluorescein unit in the measured substance will be quenched by graphene because of the energy transfer from fluorescing into graphene [24]. Recently, Eider Aparicio-Martinez et al. reported that the Ag@Graphene composites were due to their easy synthesis of Ag NPs, their excellent plasmonic properties, and the cooperation effect of the two materials in signal enhancement [25]. Moreover, through laser modification, its composite structure showed high SERS activity, and it allowed rapid detection of Rh 6G. This research can solve the above problems to a certain extent. However, in the process of actual preparation, lattice defects such as vacancy and the oxygen-containing group will inevitably occur, so that these performance indexes are much lower than the theoretical values [26,27].

In this study, Ag/C bilayer film was designed based on the above, and carbon was used to replace graphene to reduce the loss in the

* Corresponding author.
E-mail address: rjhong@usst.edu.cn (R. Hong).

https://doi.org/10.1016/j.optmat.2021.111728
Received 25 May 2021; Received in revised form 1 October 2021; Accepted 22 October 2021
Available online 8 November 2021

Table 1
Laser scanning parameter.

Parameter	Unit	Value
Laser	W	8
Beam diameter	mm	0.01
Pulse width	ns	200
Frequency	kHz	45
Scanning line spacing	mm	0.01
Scanning rate	mm/s	500–2500

preparation process, and the method was cost-effective. The surface of thin films was then modified by pulsed laser. The LSPR efficiency of the Ag/C samples can be valid adjusted by changing the laser scanning rate. The laser modification has a significant impact on the sample composition, surface, optical absorption, and SERS performance. Also, the electric field distribution of the sample has been well verified in the FDTD technique.

2. Experiment

Electron-beam evaporation was used to be fabricate the Ag/C bilayer films on BK9 substrate through high purity Ag target (99.9%) and Carbon target (99.9%). The thickness of bilayer film is 100 nm monitored via quartz crystal microbalance (thickness of Ag and C is 90 nm and 10 nm, respectively). In this work, a pure Ag film (100 nm) was also fabricated as a reference. All depositions are performed in a vacuum (less than 5×10^{-4} pa). And next, cover the blank BK9 substrates on the surface of the film when the deposition is over. Then, These films were modified by an Nd:YAG fiber pulsed laser at 1064 nm with 8 W laser power and 200 ns pulse width under the environmental conditions. The laser parameters are shown in Table 1. The scanning rate was set at 500 mm/s、1000 mm/s、1500 mm/s、2000 mm/s、2500 mm/s , respectively. These samples were defined as S1–S5 (Ag/C samples) and S1′-S5′(Ag samples), respectively. Fig. 1 shows the schematic for the experiment process.

X-ray diffraction (XRD, Miniflex600 system) and double beam spectrophotometer (Lambda1050, Perkins Elmer) were used to analyze the phases and optical absorption of samples. Observe the surface topography with an atomic force microscope (XE-100 Park system, AFM) and a scanning electron microscope (Merlin compact, Carl Zeiss, SEM). Thermo Scientific Escalab 250Xi (XPS) was used to study the composition of the samples. Raman signals was measured by the XploRA PLUS Raman spectroscopy excited by a 638 nm laser.

3. Results and discussion

3.1. Structural and properties

The XRD θ/2θ diffraction features for Ag and Ag/C films before and after laser ablation were shown in Fig. 2. Two diffraction peaks at 38.6° and 44.8° can be observed in both single Ag film and Ag/C composite thin films, corresponding to the (111) and (200) crystallographic plane of silver (JCPDS: 04–0783) in Fig. 2(a). Compared to that of a single Ag film, crystallinity of Ag/C composite film was improved due to the immobilization of Ag by carbon film [28,29]. This phenomenon causes Ag's diffraction peak in the Ag/C composite film to be stronger than that of the Ag film. Generally speaking, since these crystal planes exhibit minor surface free energy, for non-epitaxial deposition on the substrate, the film surface tends to be (001) and (111) planes [30]. Also, the thin thickness of the carbon film may lead to poor crystallinity, so there is no pronounced diffraction signal of carbon. According to Fig. 2(b), XRD diffraction features of Ag samples and Ag/C samples with the different laser rates (1000 and 2000 mm/s), respectively. Compared with before laser ablation, the diffraction intensity of samples after laser ablation is

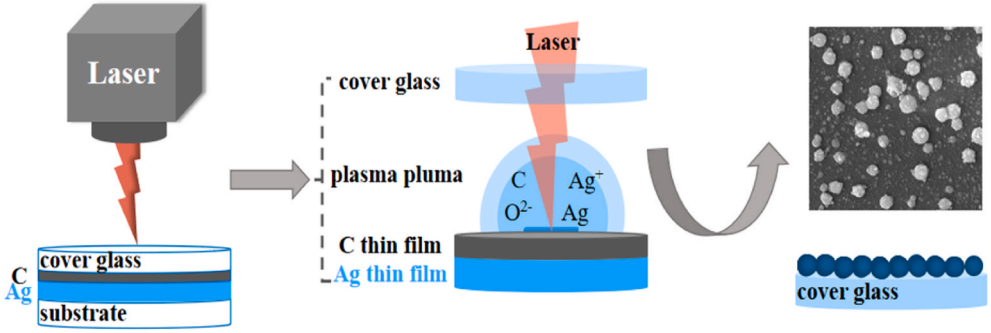

Fig. 1. The schematic for the experiment process.

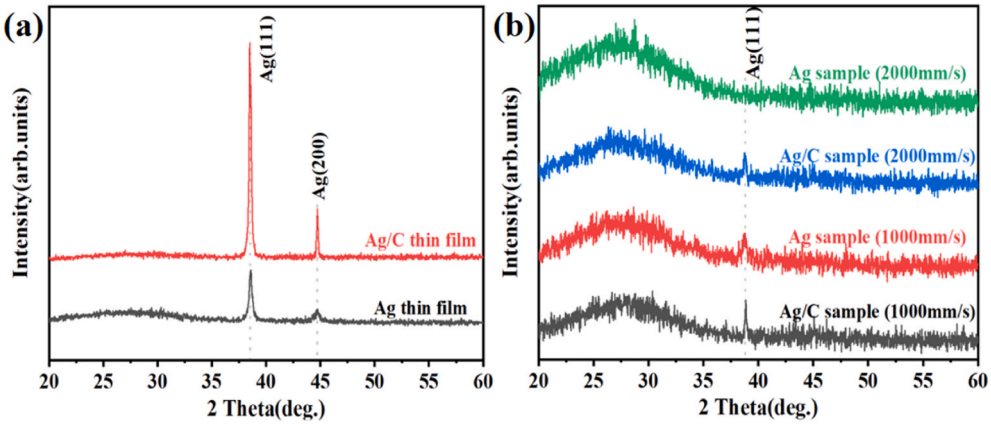

Fig. 2. XRD for Ag film and Ag/C film before (a) and after laser ablation (b).

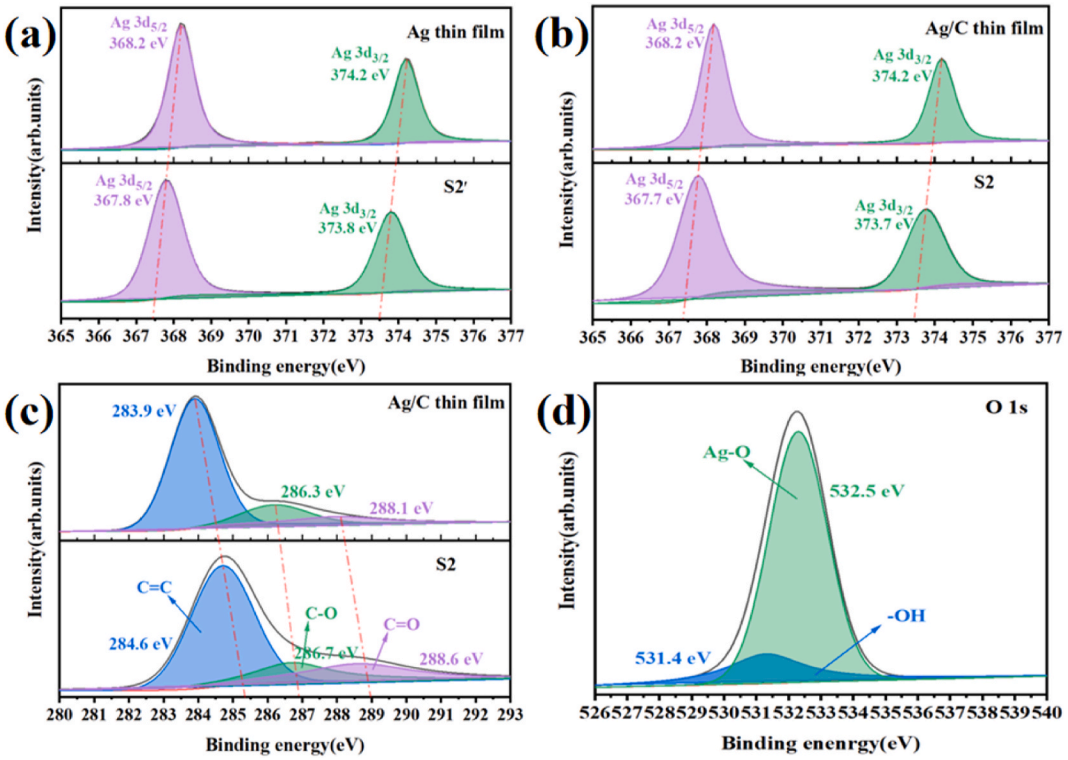

Fig. 3. XPS spectra of (a–b) Ag 3d for Ag film, S2′(1000 mm/s), Ag/C bilayer film and S2(1000 mm/s), (c) C 1s for Ag/C bilayer film and S2(1000 mm/s), (d) O 1s for S2(1000 mm/s).

significantly reduced, caused by the thinning of film thickness. Meanwhile, there is no obvious peak-shift before and after laser ablation. Under the same laser scanning rate, the diffraction peak intensity of the Ag/C sample is stronger than that of the Ag sample, which is due to the immobilization of the dispersed Ag nanoparticles on the nano-carbon. Moreover, due to the poor crystal quality, no apparent oxide phase was observed in samples.

3.2. Composition and valence states

From Fig. 3, we could see the XPS spectra of samples before and after laser ablation. The films and samples' shape and valence are in good agreement with those reported in the literature. According to Fig. 3(a), two peaks were found in the Ag film at about 368.2 eV and 373.2 eV, which are $3d_{5/2}$ and $3d_{3/2}$ of Ag atoms [31], and same as Ag/C film in Fig. 3(b). The Ag $3d_{5/2}$ and Ag $3d_{3/2}$ peaks appearing at 367.8 eV and 373.8eV are observed in S2' (Ag sample with the scanning rate of 1000 mm/s). Those peaks correspond to oxidation states such as AgO [32,33]. Meanwhile, in S2, the peaks situated at 367.7 eV and 373.7 eV responded to Ag^{+}, which indicates the formation of AgO after laser ablation [34]. As exhibited by Fig. 3(c), for Ag/C film, the C 1s spectrum can be deconvoluted into three individual peaks with binding energies of 283.9 eV, 286.3 eV, 288.1 eV. These peaks were assigned to C═C, C–O, C═O, respectively [33,35]. These peaks intensity of 286.3 eV and 288.1 eV were significantly weaker than that of 283.9 eV, which indicates that a small number of C–O bonds and C═O doubts bonds in the carbon matrix. Furthermore, compared with the Ag/C film, the binding energy of the C═C, C–O, C═O corresponding to 284.6 eV, 286.7 eV, 288.6 eV in S2, respectively. The full width of the half-maximum of the peak at 288.6 eV is slightly increased in S2, and the binding energy is generally increased. The sharp peak at 284.6 eV corresponds to the sp^2 carbon atoms, which indicates the presence of graphitic carbon [36]. In Fig. 5 (d), the O 1s spectrum of S2 can be deconvoluted into two individual peaks at 531.4 eV and 532.5 eV, respectively. The former is attributed to hydroxyl, and the latter is the Ag–O bond in the AgO structure [35,37], indicating the presence of AgO in the samples.

3.3. Surface morphology

Fig. 4(a-d) respectively shows the AFM images of the sample before and after laser ablation. The gross morphology of the Ag film or Ag/C composite film are smooth. The RMS surface roughness (Rq) Ag film and Ag/C film are 1.875, 1.920, respectively. After laser modification, however, NPs decomposes from the film's surface due to thermo-elastic force. It adheres to the cover glass, thereby forming an ordered spherical structure on the cover glass [34]. With the laser scanning rate increases, the working time of the laser on the film is reduced, the thermal interaction time is reduced and finally leads to the gradual increase of the surface roughness of the sample. As exhibited by Fig. 4(e), the RMS surface roughness (Rq) value of the Ag film and samples are 1.875, 10.351, 14.013, 21.347, 27.058, and 38.143 nm, respectively. The same trend was observed for Ag/C film and samples, and the RMS surface roughness (Rq) value of the Ag/C film and ablated samples are 1.920, 9.979, 10.799, 11.610, 13.692, and 15.473 nm, respectively, in Fig. 4(f). However, at the same rate, the surface roughness of the Ag sample is much larger than that of the Ag/C sample. As a carbon film, the covers the outer surface of the Ag/C thin film. When the same laser is irradiated on the film, part of the laser energy will be offset, resulting in a relatively gentle increase in Ag/C samples' roughness. Simultaneously, the nano-carbon covering the surface of Ag nanoparticles is not considered, so the roughness is relatively low.

Fig. 5 shows the corresponding SEM images of samples of before and after laser ablation. Laser ablation has a vital influence on the morphology of the material. Fig. 5(a) and **(c)** are SEM images for Ag film and Ag/C film, respectively. The surface morphology of the film presents a continuous structure. However, after laser ablation with a scan rate of 1000 mm/s, the structure becomes discontinuous, and nanoparticles with an ellipsoidal structure, as shown in Fig. 5(b) and **(d)**. Meanwhile, it can be intuitively found that the nanoparticle spacing of the Ag/C sample is smaller than that of the Ag sample, and the size of

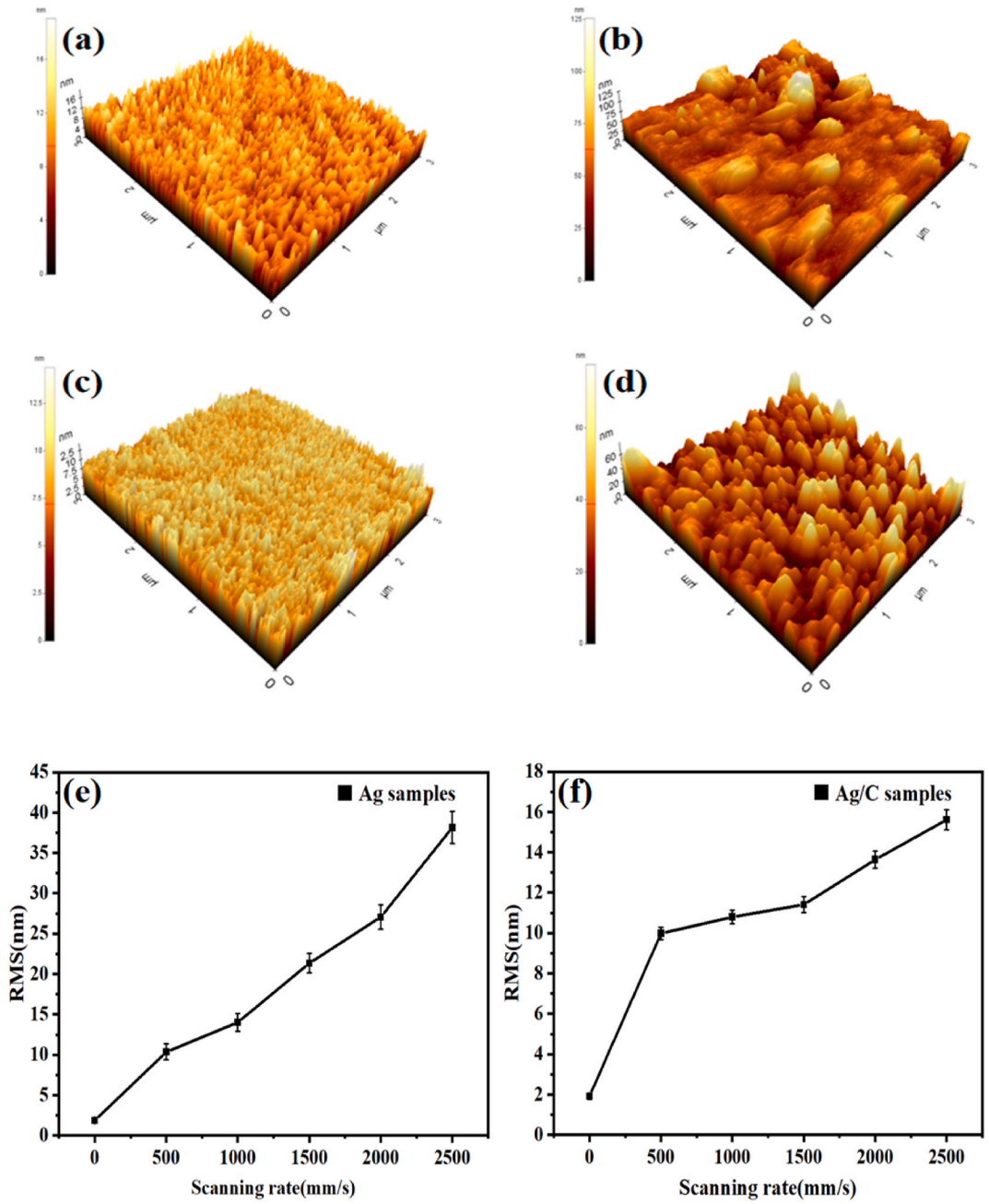

Fig. 4. AFM images of (a) Ag film, (b) Ag sample of 1000 mm/s, (c) Ag/C bilayer film, (d) Ag/C sample of 1000 mm/s (e) The surface roughness of Ag and samples, (f) the surface roughness of Ag/C and samples.

nanoparticles is larger than that of Ag samples. The inset diagram in Fig. 5(d) shows the graphitic carbon covering the sample surface. In addition, the element distributions (EDS) spectra of the films and samples are shown in Fig. S1.

3.4. Optical absorption

The absorption spectra of Ag samples were shown in Fig. 6(a), and the inset shows the absorption spectrum of Ag film. Meanwhile, in Fig. 6 (c), the absorption spectra of Ag/C samples, the inset shows the absorption spectrum of Ag/C film. Compared with Ag film, the absorption spectrum of Ag/C film has a wider absorption band. The resonance absorption intensity of the two is stronger than that of the sample after laser ablation. Before laser ablation, the film structure is continuous. It has a broad absorption peak and a stronger absorption intensity [38]. However, localized electronic coherent oscillation occurs on the sample's surface after laser ablation, which leads to the appearance of a resonance absorption peak. As the laser scanning rate increases, the wavelength of the absorption peak corresponding to the Ag sample also shows a regular shift in the infrared direction from 428 nm to 486 nm, and absorption peak intensity decreases accordingly. As shown in Fig. 6 (b), each inflection point corresponds to the wavelength of the maximum value of per curve in Fig. 6(a), which is 428 nm, 442 nm, 462 nm, 474 nm, and 486 nm, respectively. For Ag/C samples, however, the trend is similar to that of Ag samples. We can see from Fig. 6(c) that the corresponding absorption peak wavelength has a significant red shift, and absorption intensity gradually decreases. As shown in Fig. 6(d), each point in the graph indicates the wavelength corresponding to the maximum value per absorption curve, which is 457 nm, 492 nm, 497 nm, 505 nm, and 527 nm, respectively.

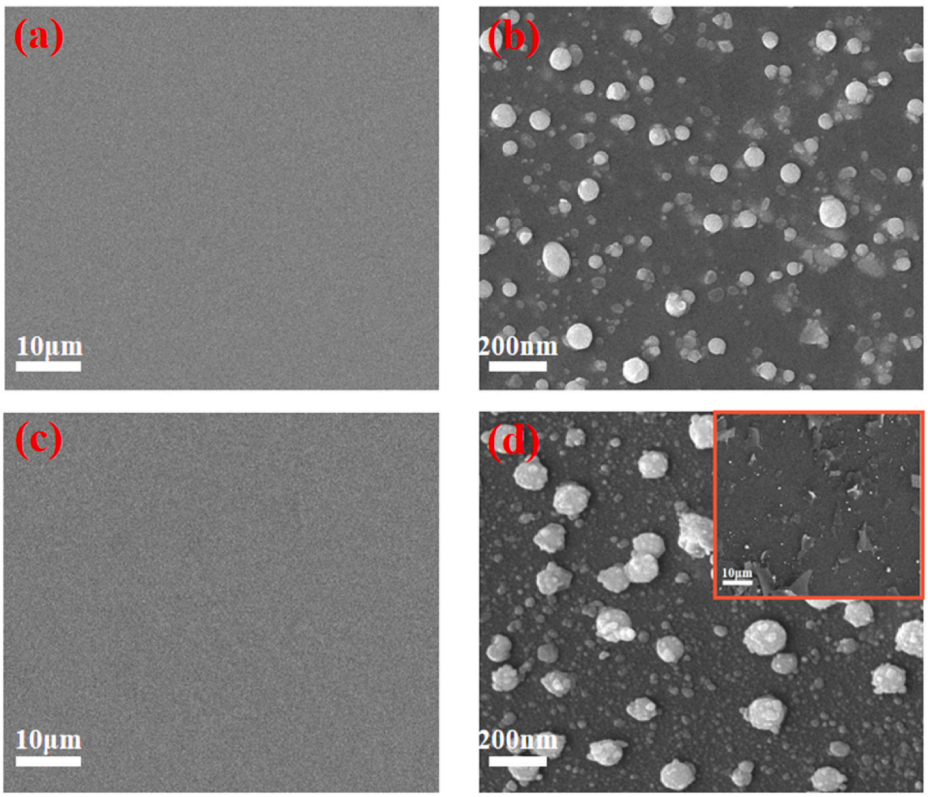

Fig. 5. SEM images of (a) Ag film, (b) Ag sample with laser scanning rate of 1000 mm/s, (c) Ag/C bilayer film, (d) Ag/C sample with laser scanning rate of 1000 mm/s and the inset shows the Ag film modified with nano-carbon.

At the same scanning rate, the Ag/C sample shows a stronger absorption intensity than the Ag sample, which is due to the larger nanoparticles of the Ag/C sample. The absorption intensity is also consistent with the tendency of the diffraction peak in XRD (Fig. 2). Under laser ablation, the continuous film transforms into a discontinuous nanoellipsoid structure so that these samples have a stronger LSPR effect. Moreover, the wavelength of the plasmon is affected by the size and shape of the particle, which is consistent with the quasi-static theory–calculating the light absorption of NPs in the ellipsoidal structure [39]. When the sample is irradiated perpendicularly by the laser, the spacing between NPs becomes smaller, resulting in a strong coupling induction [40]. This series of reasons make the absorption curve of the Ag/C sample show a more pronounced shift and broader range in the infrared direction than that of the Ag sample. This phenomenon is consistent with the effect shown by the surface morphology of the sample (Fig. 5 (a)–(d)). Moreover, the XRD and XPS results show that the laser scanning rate change causes the transformation of the sample's local dielectric environment [32]. The Drude model proposed that the refractivity of environmental medium also affects the LSPR wavelength [41]. With the oxidation of NPs surfaces, the dielectric coefficient of surrounding medium increases, and LSPR moves to the infrared direction accordingly [42]. To some extent, the thermal interaction time of the film can be reduced by increasing the laser scanning rate, resulting in the reduction of the absorption intensity. Moreover, for Ag/C samples, there is a narrow absorption band in the ultraviolet wavelength region. These peaks corresponding to the optical absorption of interband tran-sitions [43].

3.5. SERS performance

To investigate the potential influence of laser scanning speed on plasma characteristics. Rh 6G (10-5 mol/L) was used as a probe molecule to study the SERS of samples. Fig. 7 (a) and **(c)** show the Raman spectra of Ag samples and Ag/C samples, respectively. There are four strongest Raman peaks observed at about 618, 1311, 1360, and 1507 cm^{-1}, respectively. The peak of 618 cm^{-1} is the tensile vibration peak in the surface of the oxacene ring, while those peaks of 1311, 1360, and 1507 cm^{-1} are the stretching vibration peak of the C═C bond on the benzene ring [44]. As the laser scanning speed increases, the Raman intensity of the sample increases significantly. Fig. 7(b) and **(d)** show the relationship between the change of Raman intensity and the substrate number in Fig. 7(a) and **(c)** at 1507 cm^{-1}. Meanwhile, at the same scanning rate, the Ag–C composite film ablative sample's Raman strength was stronger than Ag. Obviously, the SERS of the sample can be affected by adjusting the laser scanning rate.

In general, the enhancement of the electromagnetic field plays a crucial role in enhancing SERS, and the enhancement of the electromagnetic field mainly depends on the effect of LSPR. About the absorption curve (Fig. 6), all samples showed a significant LSPR effect, leading to increased Raman signal strength. With the increase of the laser scanning rate from 500 to 2500 mm/s, the LSPR peak of the Ag–C sample was closer to the wavelength of the Raman excitation laser than that of the Ag sample, thus showing a stronger SERS effect. Documented evidence, the fluorescence of molecules was quenched by using graphene as SERS substrate. For Rh 6G attached to graphene, the fluorescence background is significantly reduced, and the Raman signal is more easily resolved [45]. Also, through laser modification of Ag@graphene composites, relatively high SERS activity was obtained, and Rh 6G could be rapidly detected. Meanwhile, the above experiments proved that Ag/C composite thin films had a good SERS effect after being modified by laser and proved the feasibility of replacing graphene with carbon. Fig. 7(e) shows the Raman intensities of the Ag/C sample and Ag sample with different days. Fig. 7(f) corresponds to the histogram of Raman intensity in Fig. 7(e). Evidently, the Raman intensity of the Ag sample decreased slightly, while that of the Ag/C sample was almost unchanged after days. Therefore, the stability of Ag/C samples is better than that of

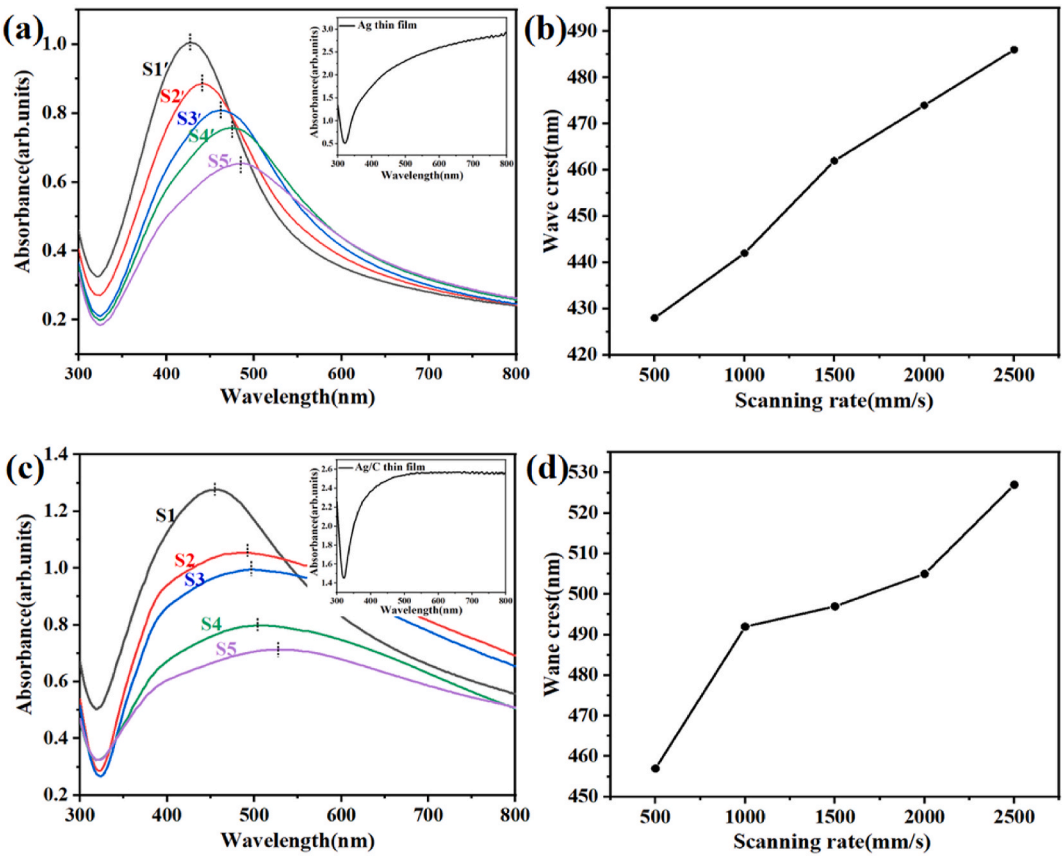

Fig. 6. Optical absorption spectra of (a) Ag samples with various laser scanning rate, the inset at the top shows optical absorption spectra of Ag film, (c) Optical absorption spectra of Ag/C samples with various laser scanning rate, the inset at the top shows optical absorption spectra of Ag/C bilayer film. Curve of wave crests of (b) every absorption spectrum of Ag samples, (d) every absorption spectrum of Ag/C samples.

Ag samples.

To research the repeatability and uniformity of the sample, the Raman signal intensity of the 1507 cm^{-1} peak was selected as a reference. In the case of a laser scanning rate of 2500 mm/s, five Ag samples and five Ag–C samples were measured by the same method. Meanwhile, the Raman intensity of the sample at 1507 cm^{-1} after several days was also compared accordingly. The relative standard deviation of the measured values of all samples is less than 3%, which indicates that the Raman intensity of the samples is basically the same [32]. In addition, the Raman signal intensity of different batches of samples is almost the same, which indicates that the samples prepared in the experiment have good uniformity and repeatability. Fig. 8 shows the intensity errors bars of the Raman peak at 1507 cm^{-1} for samples, corresponding to Fig. 7 (b), **(d)** and **(f)**. Moreover, to verify the reproducibility of the SERS spectrum. As shown in Fig. 9, 15 points were randomly selected in the Ag/C sample with a laser scanning rate of 2000 mm/s. The relative standard deviation of the measured values of all samples is less than 10%, indicating that the samples have good uniformity and reproducibility [46–48].

To further evaluate the sensitivity detection of the Ag/C substrates, the changes of SERS signal intensity at different R6G concentrations were compared. Meanwhile, compare and analyze the experimental enhancement factor (EF_e) and the theoretical enhancement factor (EF_t) [49–51], we choose the Ag/C sample with the Raman characteristic peak at 1507 cm^{-1} under 1000 mm/s. The SERS EF_e and EF_t was calculated according to the following formula :

$$EF_e = \frac{I_{SERS} C_0}{I_0 C_{SERS}} \quad (1)$$

$$EF_t = \frac{|E_{out}|^4}{|E_0|^4} \quad (2)$$

Where I_{SERS} and I_0 represent the Raman intensity for 1×10^{-12} M of R6G on the Ag/C sample and 1×10^{-5} M of R6G on BK9, and C_{SERS} and C_0 indicate the corresponding R6G concentration. E_0 is the intensity of the incident electric field, and E_{out} is the intensity of the electric field outside the NPs. In additional, Fig. 10(a) shows the change of SERS signal intensity from 10^{-5} M to 10^{-12} M R6G concentration. With the concentration of R6G decreases, even when the concentration is as low as 10^{-12} M, the SERS signal can be clearly observed. Fig. 10(b) shows the Raman intensity of I_0 and I_{SERS}. The EF_e value is calculated as high as 1.35×10^7. The maximum local electric field is 59.1 V/m, and the EF_e is 1.22×10^7. The simulation structure matches the experimental results.

In order to study the influence of the laser scanning rate on the electric field of the sample, the electric field distribution of some samples was simulated using the FDTD technique (Fig. 11). The x-y surface of the sample is irradiated vertically with a 638 nm laser and polarized along the y axis [4]. According to the prepared film thickness parameters, Ag film 100 nm and Ag/C double-layer film (Ag 90 nm, C 10 nm) were performed by FDTD simulation on the film surface. After laser processing, according to the SEM images, the size of Ag/C composite NPs was set to 100 nm and the size of Ag particles was set to 80 nm. The FDTD simulation of particles of other sizes is shown in Fig. S2. Fig. 11 (a) and **(c)** show the electric field distribution of the continuous Ag thin film and the electric field distribution at the junction of the Ag film and the carbon film. Due to the continuity of the film surface, the electric field strength of the film is weak, and there is almost no difference between the two. Fig. 11 (b) and **(d)** are the electric field distributions of Ag

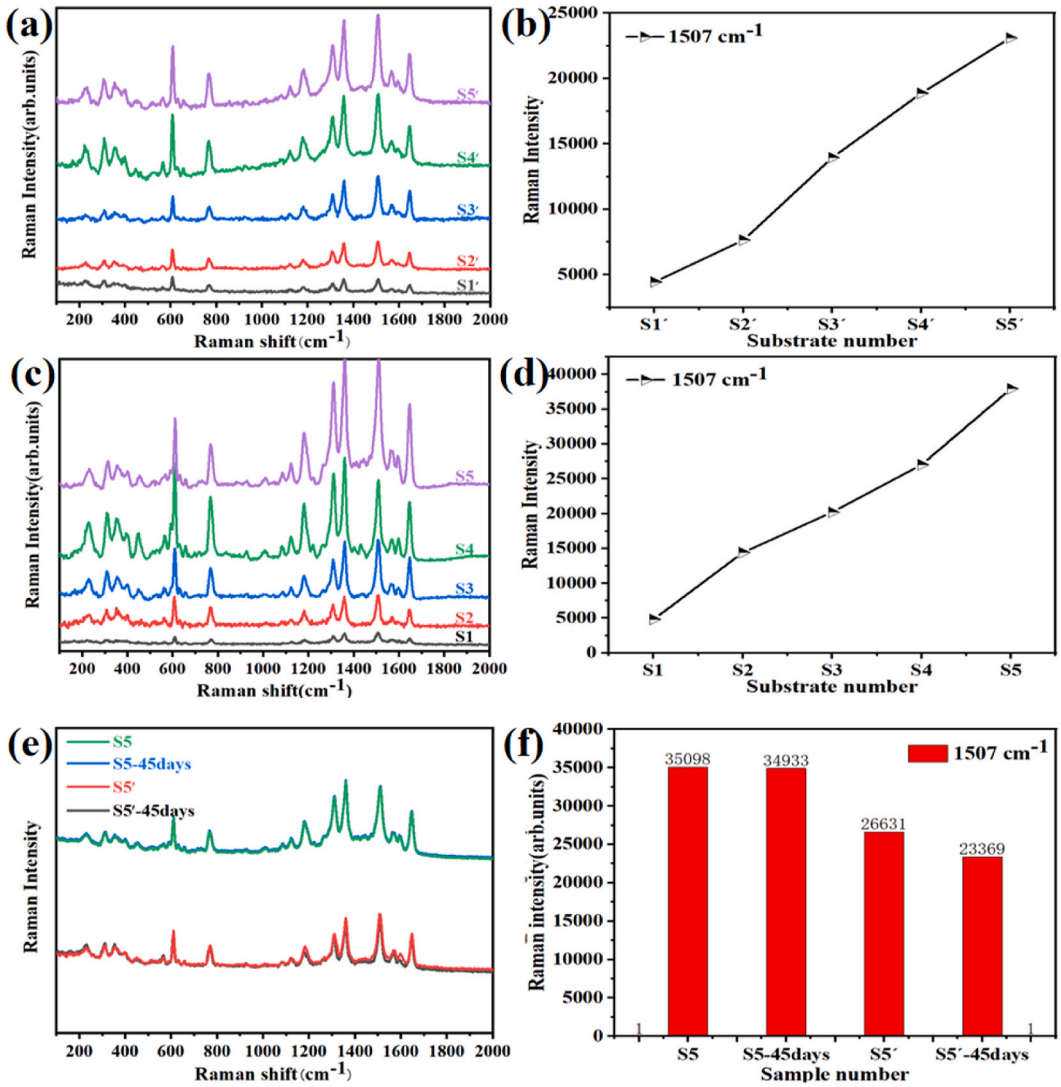

Fig. 7. SERS spectra of Rh 6G (10^{-5} M) on (a) Ag samples and (c) Ag/C samples with laser scanning rate from 500 to 2500 mm/s (b) and (d) corresponds to the Raman strength of the sample in (a) and (c) at 1507 cm^{-1}. (e) SERS spectra of Rh 6G (10^{-5} M) on Ag sample and Ag/C sample at different days. (f) The Raman intensity histogram of different samples at 1507 cm^{-1} corresponding to (e).

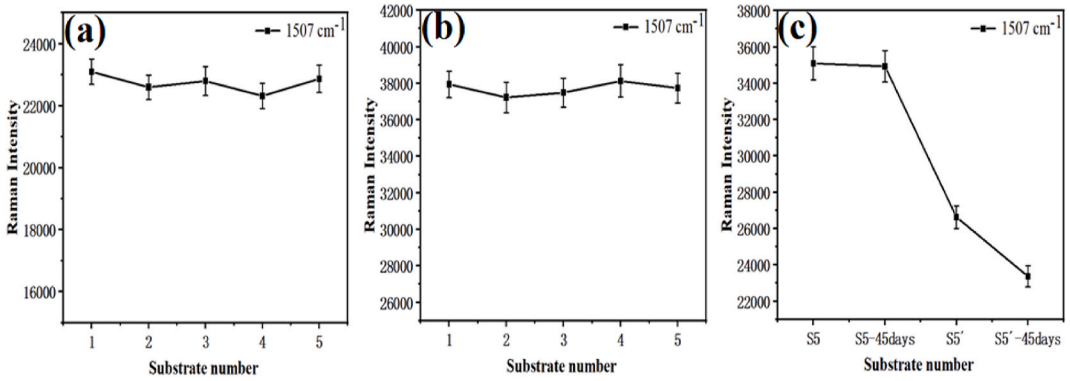

Fig. 8. The errors bars of intensity for 1507 cm^{-1} on (a) five different Ag samples, (b) five different Ag/C samples at 2000 mm/s, and (c) Raman intensity after 45 days at 2500 mm/s.

sample (1000 mm/s) and Ag/C sample (1000 mm/s), respectively. SEM images can be seen that Ag/C samples can obtain large size NPs under the same laser scanning rate. It can be seen from the simulation results that the Ag/C sample shows a stronger electric field intensity than the Ag sample, which explains the consistency of the above-mentioned SERS effect. We attribute the enhancement of the SERS signal intensity to the

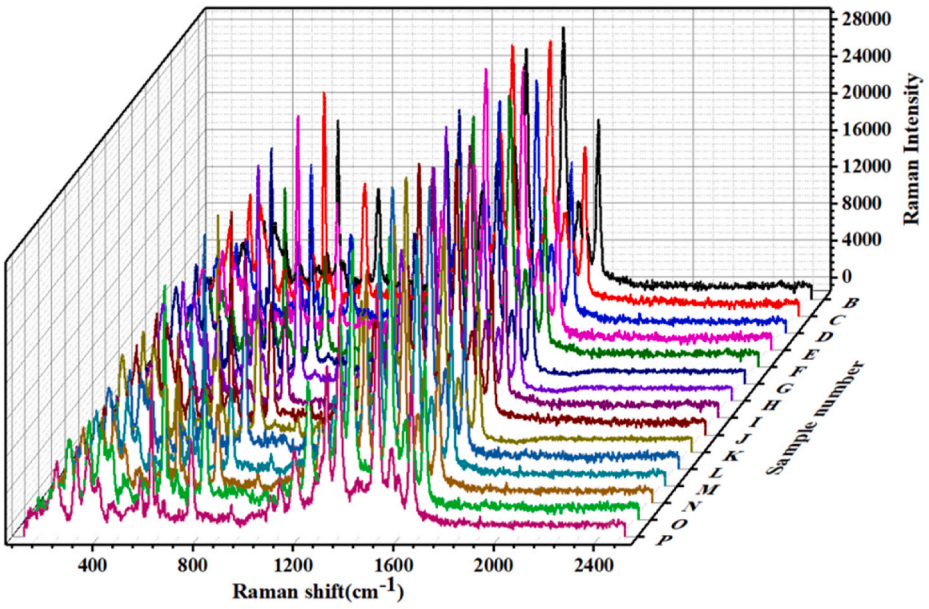

Fig. 9. SERS (Raman mapping) spectra collected at 15 spots selected randomly on Ag/C samples with 2000 mm/s.

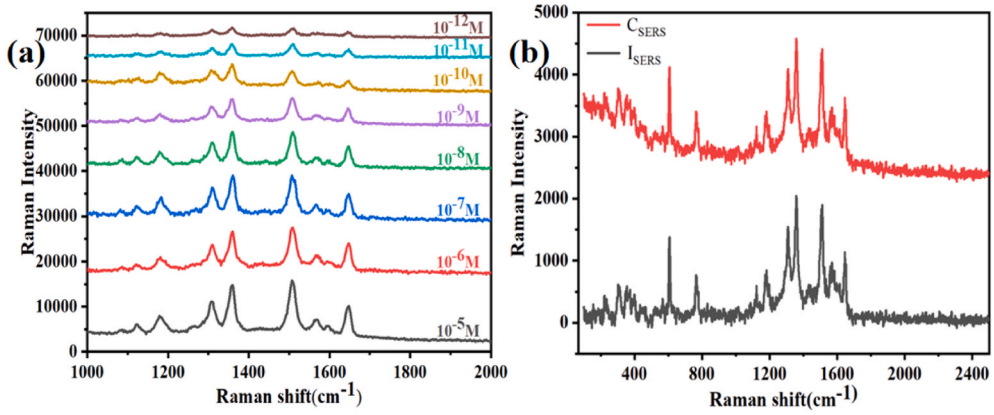

Fig. 10. (a) SERS spectra of different concentrations of R6G molecules (10^{-5}-10^{-12}) on Ag/C sample at 1000 mm/s.

accumulation of plasmonic NPs on the substrate, which ultimately led to the existence of a large number of "hot spots". The place where the red color gathers in the picture is the ''hot spot'', which represents the enhancement of the electric field. Comparing the simulation results and the experimental results, it can be found that both are in good agreement.

4. Conclusions

This experiment is improved basis on predecessors. The Ag/C thin film was prepared by substituting carbon for graphene. The SERS performance of silver thin films decorated with carbon nanoparticles tuned by laser modification at diverse laser scanning rates has been studied. The results show that the LSPR wavelength of the Ag thin film decorated with carbon nanoparticles has a significant red-shift with the continuous increase of the laser scanning rate. The Raman scattering intensities are significantly enhanced because of the rise of the particle size, particle aggregation state, and dielectric environment of the carbon nanoparticles decorated Ag thin film. Structure stability is better than Ag as-ablated samples. These study results are in good agreement with the FDTD simulation.

CRediT authorship contribution statement

Qianbing Cheng: Writing – original draft. **Qingyou Liu:** Software. **Yikai Jiang:** Investigation. **Guohao Xia:** Investigation. **Ruijin Hong:** Review, Supervision. **Chunxian Tao:** Data curation, Formal analysis. **Qi Wang:** Data curation. **Hui Lin:** Data curation. **Zhaoxia Han:** Software. **Dawei Zhang:** Validation.

Declaration of competing interest

The authors declare that they have no known competing financial interests or personal relationships that could have appeared to influence the work reported in this paper.

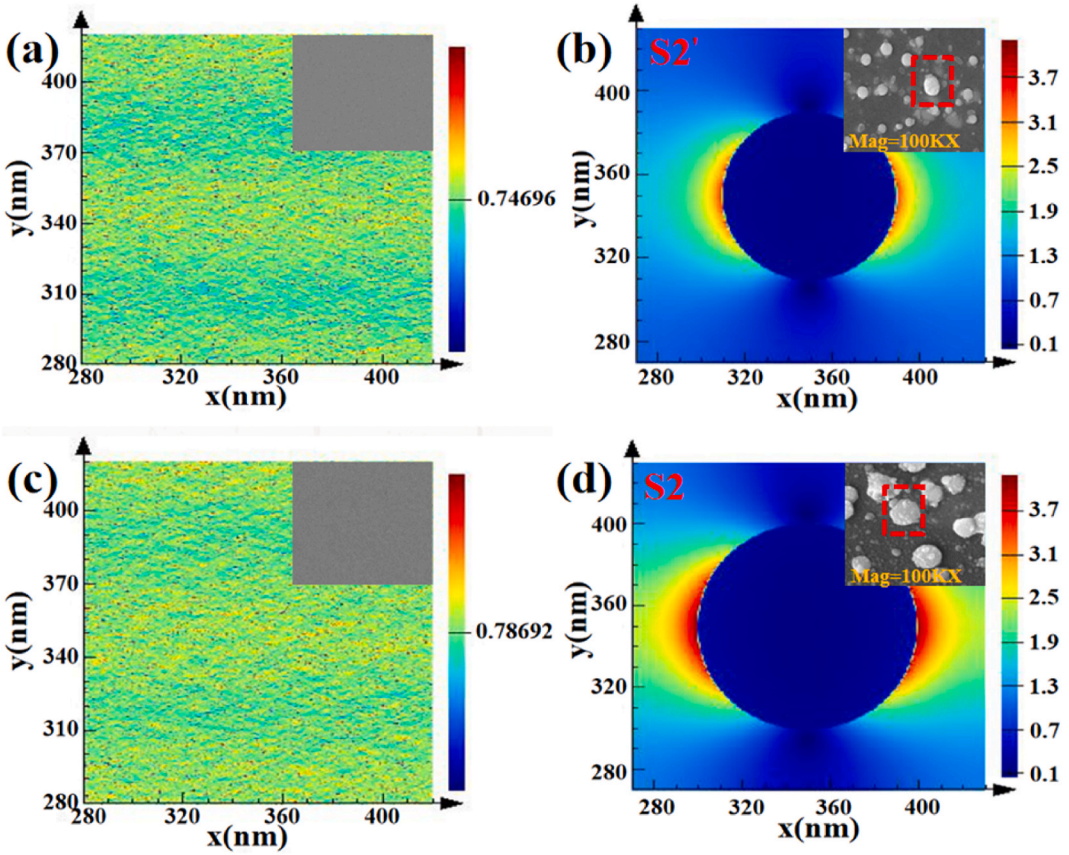

Fig. 11. FDTD simulation patterns of patterns of electric field amplitude for (a) Ag film, (b) Ag sample (S2′), (c) Ag/C film, (d) Ag/C sample (S2).

Acknowledgement

This work was supported by the National Natural. Science Foundation of China (61775141, 62075133)

Appendix A. Supplementary data

Supplementary data to this article can be found online at https://doi.org/10.1016/j.optmat.2021.111728.

References

[1] M. Moskovits, Surface-enhanced Raman spectroscopy: a brief retrospective, J. Raman Spectrosc. 36 (2005) 485–496.
[2] Y. Kalachyova, M. Erzina, P. Postnikov, V. Svorcik, O. Lyutakov, Flexible SERS substrate for portable Raman analysis of biosamples, Appl. Surf. Sci. 458 (2018) 95–99.
[3] K.P. Sooraj, M. Ranjan, R. Rao, S. Mukherjee, SERS based detection of glucose with lower concentration than blood glucose level using plasmonic nanoparticle arrays, Appl. Surf. Sci. 447 (2018) 576–581.
[4] W. Sun, R. Hong, Q. Liu, Z. Li, J. Shi, C. Tao, D. Zhang, SERS-active Ag–Al alloy nanoparticles with tunable surface plasmon resonance induced by laser ablation, Opt. Mater. 96 (2019).
[5] W. Yue, T. Gong, X. Long, V. Kravets, P. Gao, M. Pu, C. Wang, Sensitive and reproducible surface-enhanced Raman spectroscopy (SERS) with arrays of dimer-nanopillars, Sensor. Actuator. B Chem. 322 (2020).
[6] M. Dendisová, Z. Němečková, M. Člupek, V. Prokopec, EC-SERS study of phenolic acids sorption behavior on Au, Ag and Cu substrates – effect of applied potential and metal used, Appl. Surf. Sci. 470 (2019) 716–723.
[7] M. Bańkowska, J. Krajczewski, I. Dzięcielewski, A. Kudelski, J.L. Weyher, Au–Cu alloyed plasmonic layer on nanostructured GaN for SERS application, J. Phys. Chem. C 120 (2016) 1841–1846.
[8] M.K. Kinnan, G. Chumanov, Surface enhanced Raman scattering from silver nanoparticle arrays on silver mirror films: plasmon-induced electronic coupling as the enhancement, Mechanism 111 (2007) 18010–18017.
[9] R.-C. Wang, Y.-H. Chen, H.-H. Huang, K.-T. Lin, Y.-S. Jheng, C.-Y. Liu, Justification of dipole mechanism over chemical charge transfer mechanism for dipole-based SERS platform with excellent chemical sensing performance, Appl. Surf. Sci. 521 (2020).
[10] S. Kessentini, D. Barchiesi, C. D'Andrea, A. Toma, N. Guillot, E. Di Fabrizio, B. Fazio, O.M. Maragó, P.G. Gucciardi, M. Lamy de la Chapelle, Gold dimer nanoantenna with slanted gap for tunable LSPR and improved SERS, J. Phys. Chem. C 118 (2014) 3209–3219.
[11] H. Hou, P. Wang, J. Zhang, C. Li, Y. Jin, Graphene oxide-supported Ag nanoplates as LSPR tunable and reproducible substrates for SERS applications with optimized sensitivity, ACS Appl. Mater. Interfaces 7 (2015) 18038–18045.
[12] Q. Cao, K. Yuan, Q. Liu, C. Liang, X. Wang, Y.F. Cheng, Q. Li, M. Wang, R. Che, Porous Au-Ag alloy particles inlaid AgCl membranes as versatile plasmonic catalytic interfaces with simultaneous, in situ SERS monitoring, ACS Appl. Mater. Interfaces 7 (2015) 18491–18500.
[13] Y. Wang, X. Wang, X. Feng, W. Song, F. Jiang, The influence of oxygen content on the borrowing SERS activity of tin oxides/noble metal composites, Mater. Lett. 282 (2021).
[14] H. Guo, A. Zhao, Q. He, P. Chen, Y. Wei, X. Chen, H. Hu, M. Wang, H. Huang, R. Wang, Multifunctional Fe3O4@mTiO2@noble metal composite NPs as ultrasensitive SERS substrates for trace detection, Arabian Journal of Chemistry 12 (2019) 2017–2027.
[15] J. Yang, G. Song, L. Zhou, X. Wang, L. You, J. Li, Highly sensitively detecting tetramethylthiuram disulfide based on synergistic contribution of metal and semiconductor in stable Ag/TiO2 core-shell SERS substrates, Appl. Surf. Sci. 539 (2021).
[16] G. Weng, Y. Yang, J. Zhao, J. Li, J. Zhu, J. Zhao, Improving the SERS enhancement and reproducibility of inkjet-printed Au NP paper substrates by second growth of Ag nanoparticles, Mater. Chem. Phys. 253 (2020).
[17] Y. Yang, Q. Zhang, Z.W. Fu, D. Qin, Transformation of Ag nanocubes into Ag-Au hollow nanostructures with enriched Ag contents to improve SERS activity and chemical stability, ACS Appl. Mater. Interfaces 6 (2014) 3750–3757.
[18] H. Wen, H. Wang, J. Hai, S. He, F. Chen, B. Wang, Photochemical synthesis of porous CuFeSe2/Au heterostructured nanospheres as SERS sensor for ultrasensitive detection of lung cancer cells and their biomarkers, ACS Sustain. Chem. Eng. 7 (2019) 5200–5208.
[19] L. Yang, Y. Peng, Y. Yang, J. Liu, Z. Li, Y. Ma, Z. Zhang, Y. Wei, S. Li, Z. Huang, N. V. Long, Green and sensitive flexible semiconductor SERS substrates: hydrogenated black TiO2 nanowires, ACS Applied Nano Materials 1 (2018) 4516–4527.
[20] S. Sheng, Y. Ren, S. Yang, Q. Wang, P. Sheng, X. Zhang, Y. Liu, Remarkable SERS detection by hybrid Cu2O/Ag nanospheres, ACS Omega 5 (2020) 17703–17714.
[21] M.E. Ayhan, A single-step fabrication of Ag nanoparticles and CVD graphene hybrid nanostructure as SERS substrate, Microelectron. Eng. 233 (2020).

[22] P. Wang, M. Xia, O. Liang, K. Sun, A.F. Cipriano, T. Schroeder, H. Liu, Y.H. Xie, Label-free SERS selective detection of dopamine and serotonin using graphene-Au nanopyramid heterostructure, Anal. Chem. 87 (2015) 10255–10261.
[23] G. Siljanovska Petreska, M. Salsamendi, A. Arzac, G.P. Leal, N. Alegret, J. Blazevska Gilev, R. Tomovska, Covalent-bonded reduced graphene oxide-fluorescein complex as a substrate for extrinsic SERS measurements, ACS Omega 2 (2017) 4123–4131.
[24] X. Gu, G. Yang, G. Zhang, D. Zhang, D. Zhu, A new fluorescence turn-on assay for trypsin and inhibitor screening based on graphene oxide, ACS Appl. Mater. Interfaces 3 (2011) 1175–1179.
[25] E. Aparicio-Martínez, I.A. Estrada-Moreno, R.B. Dominguez, Fabrication of flexible composite of laser reduced graphene@Ag dendrites as active material for surface enhanced Raman spectroscopy, Mater. Lett. 277 (2020).
[26] Z. Zhao, P. Bai, W. Du, B. Liu, D. Pan, R. Das, C. Liu, Z. Guo, An overview of graphene and its derivatives reinforced metal matrix composites: preparation, properties and applications, Carbon 170 (2020) 302–326.
[27] P. Chen, Y. Liu, W. Zhang, J. Shang, Z. Li, Preparation of P-reduced graphene oxide composites by one-step hydrothermal method as stable electrode materials, Chem. Phys. Lett. 754 (2020).
[28] X. Yan, S. Li, J. Bao, N. Zhang, B. Fan, R. Li, X. Liu, Y.-X. Pan, Immobilization of highly dispersed Ag nanoparticles on carbon nanotubes using electron-assisted reduction for antibacterial performance, ACS Appl. Mater. Interfaces 8 (2016) 17060–17067.
[29] H. Gholamali, A. Shafiekhani, E. Darabi, S.M. Elahi, Synthesis of Ag and Au nanoparticles embedded in carbon film: optical, crystalline and topography analysis, Results in Physics 8 (2018) 336–340.
[30] I. Petrov, P.B. Barna, L. Hultman, J.E. Greene, Microstructural evolution during film growth, J. Vac. Sci. Technol. 21 (2003). S117.
[31] T. Potlog, D. Duca, M. Dobromir, Temperature-dependent growth and XPS of Ag-doped ZnTe thin films deposited by close space sublimation method, Appl. Surf. Sci. 352 (2015) 33–37.
[32] W. Sun, W. Wei, Q. Liu, T. Yan, Q. Wang, H. Lin, C. Tao, D. Zhang, R. Hong, Ag–Ag2O composite structure with tunable localized surface plasmon resonance as ultrastable, sensitive and cost-effective SERS substrate, J. Alloys Compd. 839 (2020).
[33] A.M. Ferraria, A.P. Carapeto, A.M. Botelho do Rego, X-ray photoelectron spectroscopy: silver salts revisited, Vacuum 86 (2012) 1988–1991.
[34] Y. Oh, M. Lee, Single-pulse transformation of Ag thin film into nanoparticles via laser-induced dewetting, Appl. Surf. Sci. 399 (2017) 555–564.
[35] H. Xu, J. Xie, W. Jia, G. Wu, Y. Cao, The formation of visible light-driven Ag/Ag2O photocatalyst with excellent property of photocatalytic activity and photocorrosion inhibition, J. Colloid Interface Sci. 516 (2018) 511–521.
[36] S. Yin, D. Zhao, Q. Ji, Y. Xia, S. Xia, X. Wang, M. Wang, J. Ban, Y. Zhang, E. Metwalli, X. Wang, Y. Xiao, X. Zuo, S. Xie, K. Fang, S. Liang, L. Zheng, B. Qiu, Z. Yang, Y. Lin, L. Chen, C. Wang, Z. Liu, J. Zhu, P. Muller-Buschbaum, Y.J. Cheng, Si/Ag/C nanohybrids with in situ incorporation of super-small silver nanoparticles: tiny amount, huge impact, ACS Nano 12 (2018) 861–875.
[37] Z. Li, R. Hong, Q. Liu, Q. Wang, C. Tao, H. Lin, D. Zhang, Laser patterning induced the tunability of nonlinear optical property in silver thin films, Chem. Phys. Lett. 751 (2020).
[38] S.A. Maier, Plasmonics: Fundamentals and Applications, vol. 52, Springer, 2007, pp. 49–74.
[39] H. Chen, L. Shao, Q. Li, J. Wang, Gold nanorods and their plasmonic properties, Chem. Soc. Rev. 42 (2013) 2679–2724.
[40] P.K. Jain, M.A. El-Sayed, Plasmonic coupling in noble metal nanostructures, Chem. Phys. Lett. 487 (2010) 153–164.
[41] P.B. Johnson, R.W. Christy, Optical constants of the noble metals, Phys. Rev. B 6 (1972) 4370–4379.
[42] T.R. Jensen, M.D. Malinsky, C.L. Haynes, R.P. Van Duyne, Nanosphere lithography: nanosphere lithography: tunable localized surface plasmon resonance spectra of silver nanoparticles, J. Phys. Chem. B 104 (2000) 10549–10556.
[43] B. Balamurugan, T. Maruyama, Size-modified d bands and associated interband absorption of Ag nanoparticles, J. Appl. Phys. 102 (2007).
[44] J. Lin, G. Guan, W. Yang, H. Fu, The enhanced Raman scattering of Ag nanoparticles decorated on the carbon nanotube via a simple manipulation, Opt. Mater. 95 (2019).
[45] Y. Meng, X. Yan, Y. Wang, A simple preparation of Ag@graphene nanocomposites for surface-enhanced Raman spectroscopy of fluorescent anticancer drug, Chem. Phys. Lett. 651 (2016) 84–87.
[46] J. Zhang, X. Zhang, S. Chen, T. Gong, Y. Zhu, Surface-enhanced Raman scattering properties of multi-walled carbon nanotubes arrays-Ag nanoparticles, Carbon 100 (2016) 395–407.
[47] S.B. Jamali, M.A. Khaskheli, M.I. Abro, R. Chand, N. Rekik, H. Affan, R. Ikram, Confirming the SERS enhancement at large mapping area using self-assembly of silver nanocube at liquid-liquid cyclohexane/water interface, J. Mol. Liq. 326 (2021).
[48] W. Zhengkun, Q. Jiamin, Z. Can, Z. Yong, Z. Jie, AgNIs/Al2O3/Ag as SERS substrates using a self-encapsulation technology, Opt Express 28 (2020) 31993–32001.
[49] Y. Zeng, F. Wang, D. Du, S. Liu, C. Wang, Z. Xu, H. Wang, ZnO nanotower arrays decorated with cubic and tetrahedral shaped Ag-NPs as hybrid SERS-active substrates, Appl. Surf. Sci. 544 (2021).
[50] Q. Zhang, W. Guo, L. He, L. He, Y. Chen, X. Shen, D. Wu, A new SERS substrate of self-assembled monolayer film of gold nanoparticles on silicon wafer for the rapid detection of polycyclic aromatic hydrocarbons, Mater. Chem. Phys. 250 (2020).
[51] S. Ning, W. Zhengkun, J. Mu, Z. Jie, Flexible carbon fiber cloth decorated by Ag nanoparticles for high Raman enhancement, Opt. Mater. Express 11 (2021).